Chemical Science

Accepted Manuscript

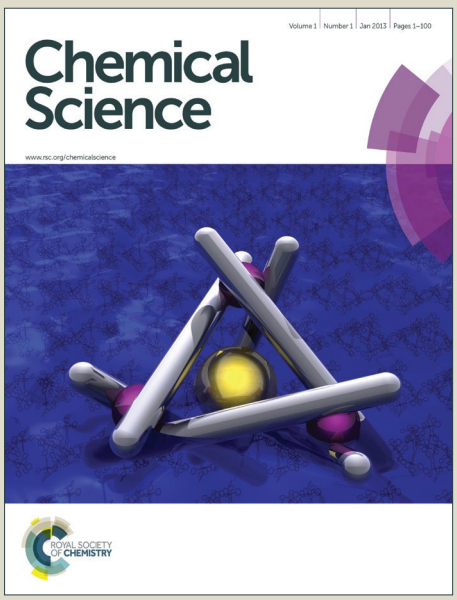

ROYAL SOCIETY OF CHEMISTRY

www.rsc.org/chemicalscience

Journal Name

ARTICLE

$[A_3X][Ga_3PS_8]$ (A = K, Rb; X = Cl, Br): Promising IR Nonlinear Optical Materials Exhibiting Concurrently Strong Second-Harmonic Generation and High Laser Induced Damage Thresholds

Bin-Wen Liu, Hui-Yi Zeng, Xiao-Ming Jiang, Guan-E Wang, Shu-Fang Li, Li Xu* and Guo-Cong Guo*

Received 00th January 20xx,
Accepted 00th January 20xx

DOI: 10.1039/x0xx00000x

www.rsc.org/

Mid-far infrared (IR) nonlinear optical (NLO) materials are of great importance in military and civil fields. However, the commercial IR-NLO crystals (such as $AgGaS_2$, $AgGaSe_2$ and $ZnGeP_2$) can't concurrently satisfy the requirements of large second-harmonic generation (SHG) and high laser induced damage thresholds (LIDTs), which seriously limited their practical applications. Here, we develop a new series of salt-inclusion chalcogenides, $[A_3X][Ga_3PS_8]$ (A = K, Rb; X = Cl, Br), which are constructed from alternate stacking of adamantane-like $[Ga_3PS_{10}]^{6-}$ cluster layers and cationic $[A_3X]^{2+}$ salt layers. Importantly, they display both large SHG responses of severalfold and high LIDTs for dozens of times that of commercial $AgGaS_2$, which exhibit the highest LIDTs among the reported IR-NLO materials that have larger SHG conversion efficiency than that of $AgGaS_2$. These properties together with wide transparent region, type I phase-matching features and congruent-melting behaviors indicate they are promising IR-NLO materials.

Introduction

Second-order nonlinear optical (NLO) materials are of current and broad interest in laser science and technology owing to their applications in producing new laser sources based on cascaded frequency conversion.[1] Many fundamental but rigorous rules are involved in selecting NLO materials for practical employment: (1) large second-order NLO susceptibility ($\chi^{(2)}$), (2) high laser induced damage thresholds (LIDTs), (3) suitable optical transparency, (4) phase-matching behavior, (5) high-quality bulk single crystals, etc. Up to now, many notable NLO crystals, such as KH_2PO_4 (KDP),[2] $KTiOPO_4$ (KTP),[3] β-BaB_2O_4 (BBO),[4] and LiB_3O_5 (LBO),[5] have been acquired. These oxide-based materials are favorably used in either the ultraviolet or visible region, but are generally restricted to apply in infrared (IR) region, owing to their short IR cutoff edge. In contrast, only few IR-NLO materials such as chalcopyrite semiconductors $AgGaS_2$ (AGS),[6] $AgGaSe_2$ (AGSe),[7] and $ZnGeP_2$ (ZGP)[8] are commercially used. They feature large NLO coefficients, but suffer from shortcomings of relatively low LIDTs, which is the main obstacle to limit their high-power laser applications. To overcome this problem, many works have been focused on designing new materials with wide band gaps,[9] which are mainly including electropositive element-inclusion chalcogenides like $LiGaS_2$,[10] $LiInS_2$,[11] $Li_2Ga_2GeS_6$,[12] and $BaGa_4S_7$,[13] metal halides like $BaClBF_4$,[14] $NaSb_3F_{10}$,[15] and $Cs_2HgI_2Cl_2$.[16] These materials show improved LIDTs; however, they come at the expense of decreasing the NLO coefficients. For instance, the Li^+ substitution for Ag^+ in the AGS leads to the finding of new IR-NLO material $LiGaS_2$, which possesses relatively higher LIDT but is afflicted with lower $\chi^{(2)}$ value of about half that of AGS. Such drawback made them not good enough for practical application. Also, most of the other IR-NLO material systems are just at the stage of laboratory research. Consequently, exploration of new material with both good NLO efficiency and LIDT is urgently needed in IR-NLO material science and laser technology.

Salt-inclusion compounds, an interesting class of host-guest materials, produces a mixed framework where species of different structures and functions can be assembled, which may lead to a new compound possessing diverse structures, improved properties, and unique functions.[17] However, prior to our investigation, the reported salt-inclusion compounds are mainly oxides that are generally unfavorable to use as IR-NLO materials. Here we extend the exploration to salt-inclusion chalcogenides, resulting in the discovery of a novel IR-NLO material system, $[K_3Cl][Ga_3PS_8]$ (**1**), $[Rb_3Cl][Ga_3PS_8]$ (**2**), $[K_3Br][Ga_3PS_8]$ (**3**), and $[Rb_3Br][Ga_3PS_8]$ (**4**), which are constructed from alternate stacking of adamantane-like $[Ga_3PS_{10}]^{6-}$ cluster layers and cationic $[A_3X]^{2+}$ (A = K, Rb; X = Cl, Br) layers along the *c* axis. Remarkably, compounds **1**-**4** exhibit concurrently large SHG responses of 4, 5, 7, and 9 times at 1064 nm (1.0, 1.1, 1.2 and 2.0 times at 1950 nm) and high LIDTs of 37, 35, 31, and 29 times that of benchmark AGS, respectively. Additionally, broad transparency range, type I phase-matching behaviors as well as congruent-melting features indicate that they are promising IR-NLO materials.

State Key Laboratory of Structural Chemistry, Fujian Institute of Research on the Structure of Matter, Chinese Academy of Sciences, Fuzhou 350002, P. R. China. E-mail: xli@fjirsm.ac.cn; gcguo@fjirsm.ac.cn

Electronic Supplementary Information (ESI) available: [details of any supplementary information available should be included here]. See DOI: 10.1039/x0xx00000x

Results and discussion

Colorless crystals of title compounds were synthesized by salt flux method with AX (A = K, Rb; X = Cl, Br) as flux agents, in which the Cl-analogues (**1** and **2**) are isostructural and crystallize in the orthorhombic space group $Pmn2_1$, while the Br-analogues (**3** and **4**) are isostructural and adopt in the monoclinic space group *Pm* (Table S1 in the Supporting Information). All of them feature a similar 2D structure formed by alternate stacking of adamantane-like $[Ga_3PS_{10}]^{6-}$ cluster layers and cationic $[A_3X]^{2+}$ layers, which exhibit hybrid frameworks with mixed covalent $[Ga_3PS_8]^{2-}$ and ionic $[A_3X]^{2+}$ salt sublattices (Fig. 1b and 1e).

In the structure of Cl-analogues, three $[GaS_4]$ tetrahedra are corner-sharing with each other to build a triangular tetrahedral trimer, on which the $[PS_4]$ tetrahedron is capping to yield form an adamantane-like $[Ga_3PS_{10}]^{6-}$ cluster (Fig. 1a). Each $[Ga_3PS_{10}]^{6-}$ cluster shares two triangular corners S(4) along the *a* direction to form a chain, which further shares the third triangular corner S(6) with the middle of triangular tetrahedral trimer in the neighboring chain along the *b* direction to create an adamantane-like $[Ga_3PS_{10}]^{6-}$ cluster layer in the *ab* plane (Fig. 1a). While the anionic layers in Br-analogues have the same conformation as those in Cl-analogues with the extending directions *a* and *b* exchanging (Fig. 1d). As listed in Tables S2 and S3, the Ga-S bond lengths and S-Ga-S bond angles in **1**-**4** are in the range of 2.225 (1) to 2.357(3) Å and 103.7(1) to 115.1(1) °, respectively. These data are respectively comparable to those in related gallium sulfides, such as $PbGa_4S_7$,[18] $SnGa_4S_7$,[19] and $Ba_4CuGa_5S_{12}$.[20] The P–S bond distances and S–P–S bond angles in **1**-**4** fall in the range of 1.994(3) to 2.112(4) Å and 105.7(1) to 113.7(1) °, respectively, which are comparable to those in $AZrPS_6$ (A = K, Rb, Cs),[21] and $K_9Nd[PS_4]_4$.[22]

The cationic $[A_3X]^{2+}$ layers in **1**-**4** can be considered as constructing from the distorted X-centered quadrangular pyramids, $[XA_5]^{4+}$, which are corner-shared with each other along the *a* and *b* directions to form an approximately coplanar with all apexes pointing along the same direction, resulting in an acentric $[A_3X]^{2+}$ layer (Fig. 1c and 1f). The cationic $[A_3X]^{2+}$ and adamantane-like $[Ga_3PS_{10}]^{6-}$ cluster layers are further anchored each other through A–S interactions (Fig. S3) to build the pseudo 3D structure, in which the adjacent layers are highly acentric in nature stacked alternately along the *c* axis lead to pack in a noncentrosymmetric (NCS) fashion.

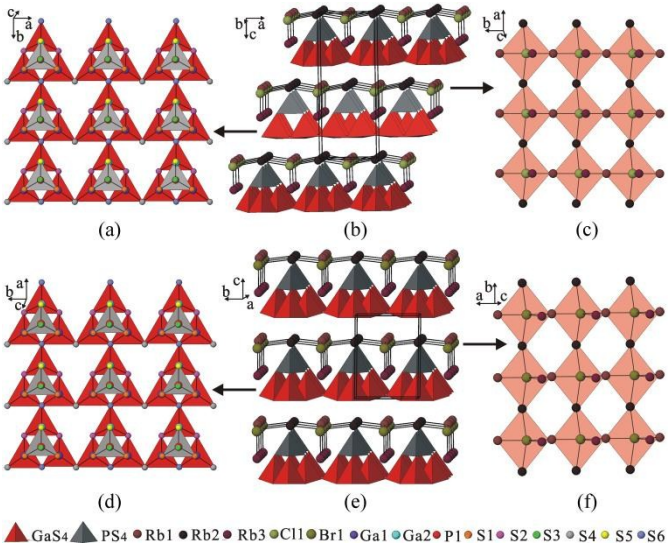

Fig. 1 $[Ga_3PS_{10}]^{6-}$ cluster layers in **2** (a) and **4** (d), cationic $[A_3X]^{2+}$ layers in **2** (c) and **4** (f), and overview of 3D frameworks of **2** (b) and **4** (e). Compound **1** is isostructural to **2** and **3** is isostructural to **4.**

Interestingly, despite having the same stoichiometric ratio and similar layer motif, Cl-analogues and the Br-analogues crystalize in different space groups, which arise from the different stacking fashions of anionic $[Ga_3PS_8]^{2-}$ layers and cationic $[A_3X]^{2+}$ layers along the *c* axis. In the Br-analogues, the neighboring $[Ga_3PS_{10}]^{6-}$ cluster layers stack along the *c* direction without transversal shift in the *ab* plane. Differently, the neighboring $[Ga_3PS_{10}]^{6-}$ cluster layers in the Cl-analogues stacked with a shift of *a*/2 along the *a* direction and a shift of 0.128*b* along the *b* direction, results in the doubling *c* axis and unit cell volume. In comparison with Cl^- (ionic radius: 1.61 Å), the larger Br^- (ionic radius: 1.82 Å) anion in X^- site make $[A_3X]^{2+}$ salt sublattices different, which further lead to the interactions between the anionic and cationic layers change, for example, the Rb(1)–S(1) interaction is weakening as evidenced by their distances increasing from 3.700 Å in **2** to 4.024 Å in **4** (Fig. S3). These variations originated from $[A_3X]^{2+}$ salt sublattices change may be responsible for the change of space group from $Pmn2_1$ of Cl-analogues to *Pm* of Br-analogues. Meanwhile, the acentric $[A_3X]^{2+}$ layer can greatly affect or directly determine the bulk acentricity, which demonstrate that ionic salt in salt-inclusion chalcogenide may act as structure directing agent to the formation of NCS compounds. These discoveries provide an enormous playground for further rational design of functional host-guest framework.

Differential scanning calorimetry (DSC) results show that compounds **1**-**4** undergo melting upon heating and crystallization upon cooling events (Fig. 2). The powder XRD patterns of the residue from one melting/recrystallization cycle are good agreement with those of the initially synthesized products and simulated ones from their CIFs (Fig. S4), indicating these phases are congruently melting. Comparing to the known IR-NLO materials, such as AGS (996 °C),[23] $LiGaS_2$ (1050 °C),[24] and $BaGa_4S_7$ (1090 °C),[13]

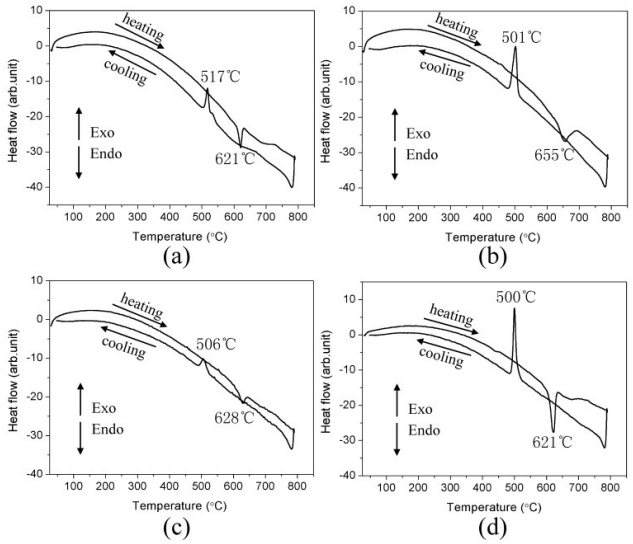

Fig. 2 DSC curves reveal the melting and recrystallization events of **1** (a), **2** (b), **3** (c) and **4** (d).

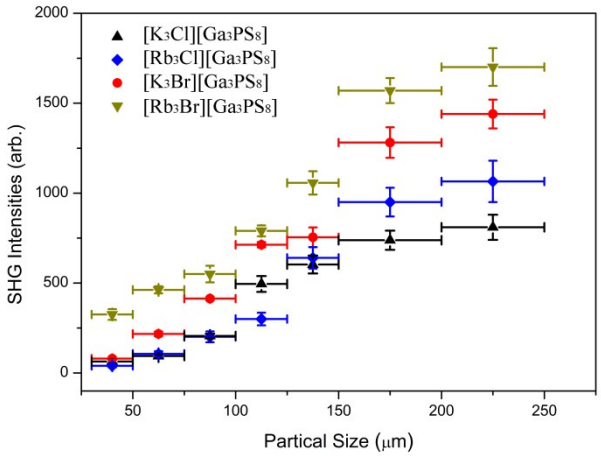

Fig. 3 Phase-matching results of **1**-**4**, the curve is to guide the eye and is not a fit to the data. The particle size deviation and the SHG intensity deviation depending on the rotation angle are respectively indicated by horizontal and vertical error bars.

compounds **1**-**4** have the relatively lower melting temperatures (621, 655, 628 and 621 °C for **1**-**4**, respectively). These results reveal that large crystals for further physical property studies can be grown using the Bridgman method at lower temperatures.

The UV−Visible−NIR diffuse reflectance spectra in Fig. S5 gives strong absorption edges at 3.60, 3.65, 3.85, and 3.50 eV for **1**-**4**, respectively, which are comparable to those Li-contained chalcogenides, such as $LiGaS_2$ (3.87 eV),[10] $Li_2Ga_2GeS_6$ (3.65 eV),[12] and Li_2CdGeS_4 (3.15 eV).[25] In comparison with the values of AGS (2.62 eV),[26] and ZGP (1.75 eV),[8] compounds **1**-**4** have relatively wider band gaps, demonstrating that they can avoid two-photon absorption (TPA) of the conventional 1064 nm incident laser and subsequently benefit improved LIDT. Further absorption spectrum in Fig. S6 shows that the absorption peak at about 609 and 530 cm^{-1} is attributed to the intrinsic absorption of P-S bond.[27] That is, there is no intrinsic absorption of chemical bonds in a broad spectral range from 0.35 to 16.5 μm (Fig. S5 and S6), suggesting that they may be suitable for a variety of NLO applications in longer wavelength regions.

Since $[GaS_4]$ and $[PS_4]$ tetrahedra are well known NLO-active building units and the cationic $[A_3X]^{2+}$ and adamantane-like $[Ga_3PS_{10}]^{6-}$ cluster layers are highly acentric in nature that pack in a NCS fashion , it can be expected that compounds **1**-**4** may achieve large SHG responses. The powder SHG measurements were carried out using a modified Kurtz powder method,[28] with lower-intensity of laser than the damage threshold of AGS. Polycrystalline AGS (d_{eff} = 18 pm/V)[29] sample was used as the reference material. The SHG intensities of **1**-**4** increase with the increasing of particle size, and then reach a relatively flat trend after a certain particle size at the incident laser of 1064 nm and 1950 nm (Fig. 3 and S7), suggesting a type I phase-matching behavior. Remarkably, compounds **1**-**4** possess large SHG signals of 4, 5, 7, and 9 times at 1064 nm (1.0, 1.1, 1.2 and 2.0 times at 1950 nm) that of AGS, respectively (Fig. S8), in which the Br-analogues exhibited stronger SHG signals, followed by the Cl-analogues.

The powder LIDT data of **1**-**4** and benchmark AGS were accessed by the single pulse powder LIDT method.[30] As illustrated in

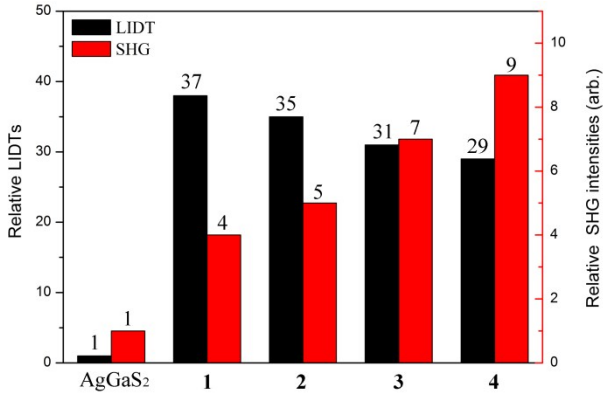

Fig. 4 The relative LIDTs and relative SHG intensities of **1**-**4** and AGS.

Fig. 4 and Table S5, the powder LIDTs of **1**-**4** are 78.5, 74.7, 64.5, and 61.2 MW·cm^{-2} at incident laser with 1064 nm, 10 ns and 1 Hz, showing 37, 35, 31, and 29 times that of AGS (2.0 MW·cm^{-2}), respectively, which are larger than those of $Ba_4ZnGa_4Se_{10}Cl_2$ (17×AGS),[31] $Pb_{17}O_8Cl_{18}$ (12.8×AGS),[32] Cu_2ZnSiS_4 (~6×AGS),[33] $SnGa_4S_7$ (19×AGS),[19] Li_2CdGeS_4 (~17×AGS),[34] Na_2BaGeS_4 (8×AGS),[35] $Na_2Hg_3Si_2S_8$ (4.5×AGS),[36] and are comparable to those of $Ba_8Sn_4S_{15}$ (26×AGS),[37] $Ba_2Ga_8GeS_{16}$ (22×AGS),[38] and Li_2MnGeS_4 (~40×AGS).[39] Importantly, it is worthy to note that compounds **1**-**4** exhibit the highest LIDTs among the IR-NLO materials that have larger SHG conversion efficiency than AGS. Their good thermal and chemical stability as well as large band gaps, which can make these phases be able to sustain laser illumination at 1064 nm without invoking TPA problems, are believed to make a significant contribution to the improvement of LIDTs. These observations indicate that compounds **1**-**4** not only exhibit strong SHG but also have high LIDTs, which should be good candidates for high-power IR-NLO applications.

To better understand the optical properties, theoretical calculations based on DFT methods were performed. The band structure calculations show that the Cl-analogues are indirect band structures with the band gaps of 2.26 and 2.36 eV for **1** and **2**, whereas the Br-analogues are direct band structures with the band gaps of 2.60 and 2.48 eV for **3** and **4**, respectively (Fig. S9). The bands can be assigned according to the total and partial DOSs in Fig. S10. For **1**-**4**, the conductive bands (CBs) close to the Fermi level are mostly composed of Ga 4s and 4p, S 3p and P 3p states, mixing with

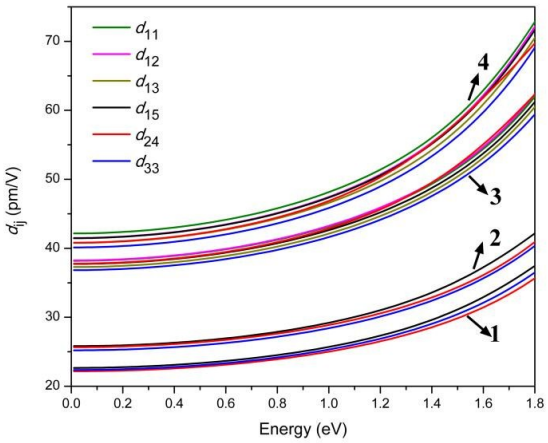

Fig. 5 Calculated frequency-dependent SHG coefficients of **1**-**4**.

small amounts of K 3p and 4s (Rb 4p and 5s) states, while the valence bands (VBs) close to the Fermi level originate predominately from S 3p and Cl 3p (Br 4p) states, therefore, their optical absorptions can mainly be ascribed to the charge transfer from S 3p and Cl 3p (Br 4p) states to Ga 4s and 4p, S 3p, P 3p and K 3p and 4s (Rb 4p and 5s) states.

To gain further insights into the NLO properties, the calculations of second-order NLO susceptibility were also performed to explain their SHG efficiencies. The calculated real part $\varepsilon_1(\omega)$ and the imaginary part $\varepsilon_2(\omega)$ of the frequency-dependent optical dielectric functions of **1**-**4** are illustrated in Fig. S11 and S12. It can be found from the dispersion of the calculated $\varepsilon_2(\omega)$ spectra that the maximum absorption peaks are located at about 5.95, and 8.36 eV for **1**; 6.01, and 8.20 eV for **2**; 5.96, and 8.07 eV for **3**; 5.57, and 7.65 eV for **4**, which are mainly contributed by the charge transfers from S 3p and Cl 3p (Br 4p) states to Ga 4s and 4p, S 3p, P 3p and K 3p and 4s (Rb 4p and 5s) states, according to the above DOS analysis. Under the restriction of Kleinman symmetry, the Cl and Br-analogues have three and six independent second-order dielectric tensor elements due to their *mm*2 and *m* point symmetry, which are related to the SHG coefficients d_{15}, d_{24}, and d_{33}; as well as d_{11}, d_{12}, d_{13}, d_{15}, d_{24} and d_{33}, respectively. As shown in Fig. 5, the calculated d_{15}, d_{24} and d_{33} are 26.7, 26.1 and 26.5 pm/V for **1**, 30.7, 30.3, 29.8 pm/V for **2**; d_{11}, d_{12}, d_{13}, d_{15}, d_{24} and d_{33} coefficients are 45.2, 45.3, 44.1, 44.6, 45.0 and 43.6 pm/V for **3**, 50.9, 50.2, 49.2, 50.1, 49.7 and 48.5 pm/V for **4**, respectively, at the wavelength of 1064 nm (1.165 eV). It shows that the calculated average NLO coefficients d_{ij} display an increasing trend with the following order: **1** (22.5 pm/V) < **2** (25.6 pm/V) < **3** (44.6 pm/V) < **4** (49.7 pm/V), which is in accordance with the experimental observations.

Conclusions

In summary, a new series of salt-inclusion chalcogenides, $[A_3X][Ga_3PS_8]$ (A = K, Rb; X = Cl, Br), have been obtained using salt flux method, which display both large SHG responses of 4-9 times at 1064 nm (and 1-2 times at 1950 nm) and high LIDTs of 29-37 times that of the benchmark AGS, as well as type I phase-matching feature. It is worthy to note that these wide band gaps compounds exhibit the highest LIDTs among the IR-NLO materials that have larger SHG conversion efficiency than AGS. Meanwhile, the high-yield, congruent-melting behavior, alone with relatively low melting/crystalizing points of all compounds make them feasible to grow large single crystals needed for practical application by the well-known Bridgman method. All these findings suggest that the title compounds can be good candidates for IR-NLO materials, and efforts to grow bulk crystals are in progress. Moreover, the current studies also show that the alkali metal halide salts in salt-inclusion chalcogenides may sever as structure directing agent to the formation of NCS compounds, which provide a new opportunity to design new structure-directing functional materials.

Acknowledgements

We gratefully acknowledge financial support from the NSF of China (91222204, 21403231, 21471149, and 21303203) and the NSF of Fujian Province (2014J05025, 2013J05034).

Notes and references

1 (a) V. A. Serebryakov, E. V. Boiko, N. N. Petrishchev and A. V. Yan, *J. Opt. Technol,* 2010, **77**, 6−17. (b) W. Chen, G. Mouret, D. Boucher and F. K. Tittel, *Appl. Phys. B: Laser Opt,* 2001, **72**, 873−876. (c) C. T. Chen and G. Z. Liu, *Annu. Rev. Mater. Sci,* 1986, **16**, 203−243. (d) P. J. Pauzauskie and P. Yang, *Mater. Today,* 2006, **9**, 36−45. (e) P. F. Bordui, M. M. Fejer, *Annu. ReV. Mater. Sci,* 1993, **23**, 321−379.

2 J. F. Ward and P. A. Franken, *Phys. Rev,* 1964, ***133***, A183−A190.

3 K. Kato, *IEEE J. Quantum Electron,* 1991, **27**, 1137−1140.

4 C. T. Chen, B. C. Wu, A. D. Jiang and G. M. You, *Sci. Sin., Ser. B* 1985, **28**, 235−243.

5 C. T. Chen, Y. C. Wu, A. D. Jiang, B. Wu, G. M. You, R. K. Li and S. J. Lin, *J. Opt. Soc. Am. B,* 1989, **6**, 616−621.

6 A. Harasaki and K. J. Kato, *Appl. Phys,* 1997, **36**, 700−703.

7 G. C. Catella, L. R. Shiozawa, J. R. Hietanen, R. C. Eckardt, R. K. Route, R. S. Feigelson, D. G. Cooper and C. L. Marquardt, *Appl. Opt,* 1993, **32**, 3948−3951.

8 G. D. Boyd, E. Buehler and F. G. Storz, *Appl. Phys. Lett,* 1971, **18**, 301−304.

9 L. Kang, M. L. Zhou, J. Y. Yao, Z. S. Lin, Y. C. Wu, C. T. Chen, *J. Am. Chem. Soc.* 2015, **137**, 13049–13059.

10 L. Isaenko, A. Yelisseyev, S. Lobanov, P. Krinitsin, V. Petrov and J. J. Zondy, *J. Non-Cryst. Solids,* 2006, **352**, 2439−2443.

11 L. Isaenko, I. Vasilyeva, A. Yelisseyev, S. Lobanov, V. Malakhov, L. Dovlitova, J. J. Zondy and I. Kavun, *J. Cryst. Growth,* 2000, **218**, 313−322.

12 Y. Kim, I. S. Seo, S. W. Martin, J. Baek, P. S. Halasyamani, N. Arumugam and H. Steinfink, *Chem. Mater,* 2008, **20**, 6048−6052.

13 X. S. Lin, G. Zhang and N. Ye, *Cryst. Growth Des,* 2009, **9**, 1186−1189.

14 M. Zhang, S. Pan, Z. Yang, Y. Wang, X. Su, Y. Yang, Z. Huang, S. Han and K. R. Poeppelmeier, *J. Mater. Chem. C* 2013, **1**, 4740–4745.

15 G. Zhang, J. G. Qin, T. Liu, Y. J. Li, Y. C. Wu and C. T. Chen, *Appl. Phys. Lett,* 2009, **95**, No. 261104.

16 G. Zhang, Y. J. Li, K. Jiang, H. Y. Zeng, T. Liu, X. G. Chen, J. G. Qin, Z. S. Lin, P. Z. Fu, Y. C. Wu and C. T. Chen, *J. Am. Chem. Soc,* 2012, **134**, 14818−14822.

17 (a) W. L. Queen, J. P. West, S.-J. Hwu, D. G. VanDerveer, M. C. Zarzyczny and R. A. Pavlick, *Angew. Chem. Int. Ed,* 2008, **47**, 3791–3794. (b) S.-J. Hwu, M. Ulutagay-Kartin, J. A. Clayhold, R. Mackay, T. A. Wardojo, C. J. O'Connor and M. Krawiec, *J. Am. Chem. Soc,* 2002, **124**, 12404−12405.

18 X. Li, L. Kang, C. Li, Z. Lin, J. Yao and Y. Wu, *J. Mater. Chem. C* 2015, **3**, 3060−3067.

19 Z. Z. Luo, C. S. Lin, H. H. Cui, W. L. Zhang, H. Zhang, Z. Z. He and W. D. Cheng, *Chem. Mater,* 2014, **26**, 2743−2749.

20 S. M. Kuo, Y. M. Chang, M. Chung, J. I. Jang, B. H. Her, S. H. Yang, J. B. Ketterson, M. G. Kanatzidis and K. F. Hsu, *Chem. Mater,* 2013, **25**, 2427−2433.

21 S. Banerjee, J. M. Szarko, B. D. Yuhas, C. D. Malliakas, L. X. Chen and M. G. Kanatzidis, *J. Am. Chem. Soc,* 2010, **132**, 5348−5350.

22 Y. Wu and W. Bensch, *Inorg. Chem,* 2008, **17**, 7523−7534.

23 B. J. Chen, S. F. Zhu, B. J. Zhao, J. J. Zhang, Y. Huang, M. Li, J. Liu, B. Tan, R. L. Wang and Z. Y. He, *J Cryst Growth*, 2006, **292**, 490−493.

24 L. Isaenko, I. Vasilyeva, A. Merkulov, A. Yelisseyev and S. Lobanov, *J. Cryst. Growth,* 2005, **275**, 217−223.

25 J. A. Brant, D. J. Clark, Y. S. Kim, J. Y. Jang, J. H. Zhang, J. A. Aitken and *Chem. Mater,* 2014, **26**, 3045−3048.

26 G. C. Bhar and R. C. Smith, *Phys. Stat. Solidi A*, 1972, **13**, 157−168.

27 C. R. Evenson IV and P. K. Dorhout, *Inorg. Chem*. 2001, **40**, 2884-2891

28 S. K. Kurtz and T. T. Perry, *J. Appl. Phys,* 1968, **39**, 3798−3813.

29 G. C. Bhar, *Jpn. J. Appl. Phys*. 1993, **32**, 653−659.
30 (a) M.-J. Zhang, X.-M. Jiang, L.-J. Zhou and G.-C. Guo, *J. Mater. Chem. C* 2013, **1**, 4754−4760. (b) M.-J. Zhang, B.-X. Li, B.-W. Liu, Y.-H. Fan, X.-G. Li, H.-Y. Zeng and G.-C. Guo, *Dalton Trans,* 2013, **42**, 14223−14229. (c) Q. Wu, X. G. Meng, C. Zhong, X. G. Chen and J. G. Qin, *J. Am. Chem. Soc,* 2014, **136**, 5683−5686. d) J. A. Brant, D. J. Clark, Y. S. Kim, J. I. Jang, A. Weiland and J. A. Aitken, *Inorg. Chem,* 2015, **54**, 2809−2819.
31 Y. Y. Li, P. F. Liu, L. Hu, L. Chen, H. Lin, L. J. Zhou and L. M. Wu, *Advanced Optical Materials,* 2015. **7**, 957−966.
32 H. Zhang, M. Zhang, S. Pan, X. Dong, Z. Yang, X. Hou, Z. Wang, K. B. Chang and K. R. Poeppelmeier, *J. Am. Chem. Soc,* 2015, **137**, 8360−8363.
33 K. A. Rosmus, J. A. Brant, S. D. Wisneski, D. J. Clark, Y. S. Kim, J. I. Jang, C. D. Brunetta, J.-H. Zhang and M. N. Srnec, J. A. Aitken, *Inorg. Chem,* 2014, **53**, 7809−7811.
34 J. I. Jang, D. J. Clark, J. A. Brant, J. A. Aitken and Y. S. Kim, *Opt. Lett,* 2014, **39**, 4579−4582.
35 K. Wu, Z. Yang, and S. Pan, *Angew. Chem. Int. Ed.,* 2016, DOI: 10.1002/anie.201602317.
36 K. Wu, Z. Yang, and S. Pan, *Chem. Mater.* 2016, **28**, 2795−2801.
37 Z.-Z. Luo, C.-S. Lin, W.-L. Zhang, H. Zhang, Z.-Z. He and W.-D. Cheng, *Chem. Mater,* 2014, **26**, 1093−1099.
38 B.-W. Liu, H.-Y. Zeng, M.-J. Zhang, Y.-H. Fan, G.-C. Guo, J.-S. Huang and Z.-C. Dong, *Inorg. Chem,* 2015, **54**, 976−981.
39 J. A. Brant, D. J. Clark, Y. S. Kim, J. I. Jang, A. Weiland, J. A. Aitken and *Inorg. Chem,* 2015, **54**, 2809−2819.